Published in final edited form as:
J Am Chem Soc. 2006 December 27; 128(51): 16834–16845. doi:10.1021/ja064859d.

Differential Sensing of Protein Influences by NO and CO Vibrations in Heme Adducts

Mohammed Ibrahim, **Changliang Xu**, and **Thomas G. Spiro***
Department of Chemistry, Princeton University, Princeton, New Jersey 08544

Abstract

Heme proteins bind the gaseous ligands XO (X = C, N, O) via backbonding from Fe d_π electrons. Backbonding is modulated by distal interactions of the bound ligand with the surrounding protein and by variations in the strength of the *trans* proximal ligand. Vibrational modes associated with FeX and XO bond stretching coordinates report on these interactions, but the interpretive framework developed for CO adducts, involving anticorrelations of νFeC and νCO, has seemed not to apply to NO adducts. We have now obtained an excellent anticorrelation of νFeN and νNO, via resonance Raman spectroscopy on (N-methylimidazole)Fe(II)TPP-Y(NO), where TPP-Y is tetraphenylporphine with electron donating or withdrawing substituents, Y, that modulate the backbonding; the problem of laser-induced dissociation of the axial base was circumvented by using frozen solutions. New data are also reported for CO adducts. The anticorrelations are supported by DFT calculations of structures and spectra. When protein data are examined, the NO adducts show large deviations from the modeled anticorrelation when there are distal H-bonds or positive charges. These deviations are proposed to result from closing of the FeNO angle due to a shift in the valence isomer equilibrium toward the Fe(III)(NO^-) form, an effect that is absent in CO adducts. The differing vibrational patterns of CO and NO adducts provide complementary information with respect to protein interactions, which may help to elucidate the mechanisms of ligand discrimination and signaling in heme sensor proteins.

Introduction

The gaseous molecules CO, NO and O_2 (XO) bind avidly to heme, thanks to effective backdonation of Fe(II) d_π electrons to their π* orbitals. Nature has harnessed this property to regulate essential biochemical processes in response to the presence of these molecules. Heme sensor proteins are the signal proteins for these regulatory mechanisms.[1] They contain an enzymatic or DNA-binding domain, linked to a heme domain. Activity is turned on or off when the appropriate ligand binds to the heme. There is great interest in understanding how the heme domain discriminates among the three XO molecules, and how the binding event is transduced into activation.

Both phenomena, discrimination and signaling, involve changes in the interactions between the heme group and the surrounding protein when the XO ligand binds. Resonance Raman spectroscopy can provide useful information about these interactions, since it can separately monitor vibrational modes of the protein, the porphyrin macrocycle, and the heme-bound ligand.

Backdonation produces anticorrelation between the X-O and Fe-X bond strengths; as backdonation increases the Fe-X bond order increases, while the X-O bond order decreases.

*To whom correspondence should be addressed. Tel.: 609-258-3907, Fax: 609-258-0348, E-mail: spiro@princeton.edu.

Negative linear correlations between the X-O stretching and Fe-X stretching frequencies have been observed for Fe(II) porphyrin adducts with all three X-O ligands.[2,3] In the case of CO, negative backbonding correlations are seen as well for six-coordinate adducts with axial base ligands.[3] However, the correlations are displaced to higher or lower CO when the axial ligand bond is weakened or strengthened, because the effect on the Fe-C bond due changes in backbonding are compensated by sigma bonding competition, leaving FeC essentially unaltered.[4]

These correlations are obeyed in CO adducts of heme proteins, as well as protein-free complexes, and have been used extensively to gauge the nature of distal polar interactions, which affect backbonding, or the weakening of the axial ligand bond via heme displacement.[4-6] However, NO adducts of heme proteins are less well behaved. Plots of νNO against νFeN are scattered, and the variation in FeN is small.[7-9] This behavior led Park and Boxer to suggest that backbonding is unimportant in heme-NO adducts, and that protein-induced electrostatic shifts in νNO (Stark effect) are associated with anharmonicity in the NO stretch.[8] As noted above, however, νNO and νFeN *are* anticorrelated for five-coordinate (5-c) Fe(II) porphyrin NO adducts, with a slope essentially the same as that observed for the corresponding CO adducts.[2] At least in these adducts, backbonding is as important for NO as it is for CO. On the other hand, vibrational data have not been available for protein-free six-coordinate (6-c) NO adducts, leaving open the possibility that backbonding is somehow vitiated by the axial ligand. Because of the strong *trans* effect in Fe(II)NO adducts, axial ligands bind weakly. We found it impossible to obtain 6-c RR spectra even at axial base concentrations sufficient to observe 6-c UV/VIS absorption spectra, and concluded that the axial ligand is dissociated by photo- and/or thermal effects of the Raman laser.[9]

Another ambiguity concerns the nature of the vibrations themselves. From nuclear resonance vibrational spectroscopy (NRVS) Sage and coworkers[10] found that the mode commonly assigned to νFeN in MbNO, at 556 cm^{-1} actually has a smaller Fe displacement than does another mode, at 451 cm^{-1}, which they suggested should be reassigned to FeN. Could the correlation problem lie in tracking the wrong mode? Because the FeNO equilibrium geometry is bent (~140°), the Fe-N stretching and Fe-N-O bending coordinates are necessarily combined into in- and out-of-phase combinations in the relevant normal modes. (The FeCO unit is essentially linear, so the mixing problem does not arise.) How much each contributes is a quantitative matter.

In this study, we re-examine these issues with fresh computations, and with new experimental data. On the computational side, we find, as have others,[11] that the adequacy of DFT calculations is sensitive to the nature of the functional. In the case of 6-c NO adducts, the σ bonding competition between NO and the trans axial ligand is difficult to capture accurately because of the strong trans labilizing effect of NO.[2] In this regard, we find that hybrid functionals do a poorer job than non-hybrid functionals, probably by introducing spin contamination. The best agreement with experimental bond-distances is given by the non-hybrid BLYP functional, and the normal modes extracted from this calculation have Fe-N stretching as the dominant coordinate for the higher of the stretch/bend modes, for both 5-c and 6-c adducts, justifying the conventional experimental assignment of νFeN.

On the experimental side, we have overcome the problem of axial base lability by freezing solutions of 6-c adducts. The frozen solution enforces efficient recombination of the photo-detached axial ligand, permitting 6-c RR spectra to be recorded. Data on 6-c adducts for a series of porphyrins having electron donor or acceptor peripheral substituents produce a well-behaved anti-correlation between NO and FeN, just as for CO adducts, albeit with different slope and different displacement from the 5-c line. Decent backbonding correlations can be computed by appending electron donor and acceptor substituents to porphine *in silico*, although the results

are less satisfactory for NO than for CO, reflecting the greater electronic complexity of the NO adducts.

When protein data are re-examined in the light of these results, it becomes evident that the scatterplots seen for NO adducts reflect deviations from the expected anticorrelation that depend on the presence of distal H-bonds or positive charges. A bonding model is developed in which these electrostatic effects diminish the FeNO angle by stabilizing the Fe(III)(NO^-) valence isomer. This model may prove useful in mapping the heme pocket interactions of sensor proteins, when both CO and NO data are considered.

Methods

Materials

Iron(III) tetraphenylporphyrin chloride, Fe(III)(TPP)Cl, and its phenyl substituted analogues (Fe(III)(TPP-Y)Cl, where Y = *p*-hydroxy, *p*-methoxy, *p*-methyl, 2,6-dicholoro, 2,6-difluoro, *p*-nitro and pentafluoro, respectively) were purchased from Midcentury Chemicals (Posen, Illinois). Some of these samples that possess fluorescing impurities were purified by treating the sample solutions with activated charcoal (EM Science, Cherry Hill, NJ). N-methylimidazole (N-MeIm) (99+ %) and methanol (99.8 %, anhydrous) were purchased from Aldrich. Methylene chloride (Optima) was purchased from Fisher Scientific. N,N-dimethylformamide (DMF, spectrophotometric grade) was obtained from J. T. Baker (Phillipsburg, NJ).

Preparation of the 6-c Fe(II)-NO Complexes

6-c NO adducts, (N-MeIm)Fe(II)TPP-Y(NO), were prepared according to the literature procedure[12] with some modifications. Specifically, to a mixture of 110 μl of N-MeIm (1.4 mmol) and 15 μl methanol (0.37 mmol) in an EPR tube was added iron(III) porphyrin stock solution in CH_2Cl_2 to make a final concentration of ~400 μM and a volume of 150 μl. The EPR tube was sealed with a septum and the solution was deoxygenated by flushing with pure nitrogen gas for ~15 min. Then, ^{14}NO gas (C.P, Matheson Gas Products Inc.), which was pre-purified by bubbling through a 2.5 M NaOH solution and water, was introduced to the sample for 5-10 minutes. The formation of 6-c Fe^{II}-^{14}NO was checked and confirmed by absorption spectroscopy (via observing subtle changes in the Q bands).

The 6-c Fe^{II}-^{15}NO complexes were prepared in a similar fashion, except that nitric oxide ^{15}NO gas was generated by reacting sodium nitrite, $Na^{15}NO_2$ (^{15}N 99 %, Icon Services, Summit, NJ), with L-ascorbic acid (Aldrich) in an anaerobic aqueous solution. The gas generated was immediately transferred, via a gas tight syringe, to the degassed porphyrin solution in the EPR tube and formation of 6-c NO adduct was checked with absorption spectroscopy.

Preparation of 6-c Fe(II)-CO Complexes

To a 5 μl of N-MeIm (63 μmol) in an EPR tube was added Fe(III) porphyrin solution (in DMF or CH_2Cl_2) to make a final concentration of ~400 μM and a volume of 150 μl. The tube was then sealed and purged with N_2 for ~15 minutes. The sample was reduced by addition of 17 mM (final concentration) of aqueous anaerobic solution of sodium dithionite ($Na_2S_2O_4$, Aldrich) via a gas-tight syringe. ^{12}CO gas (BOC Gases) was flushed into the solution for ~10 minutes to form Fe(II)-CO adducts. For the ^{13}CO analogue, the EPR tube was connected to the vacuum system, purged with N_2 gas for 15 minutes, and then evacuated; this step was repeated three times, and then ^{13}CO gas (^{13}C 99 %, Icon Services, Summit, NJ) was introduced to the sample. The formation of the 6-c Fe^{II}-CO complexes were confirmed by absorption spectroscopy.

Raman spectroscopy

RR spectra were collected at 77 K by using the 413.1 or 406.7 nm lines of the Kr ion-laser (2080-RS, Spectra Physics) via backscattering geometry. Photo-dissociation of bound N-MeIm, NO and CO was minimized by using low laser power (~0.7-1mW) at the sample. The spectra were collected with a triple monochromator (Spex 1877 Triplimate, Spex Industries, Inc.) and a liquid nitrogen cooled CCD detector (Model 7375-0001, Roper Scientific) operating at -110°C. Spectra were calibrated with dimethyl formamide, ethyl acetate and dimethyl sulfoxide-d_6 and analyzed by Grams/AI software (version 7.0, Thermo-Galactic).

Computations

Different DFT functionals were used in this study to better reproduce the experimental observations: B3LYP for heme-CO models and BLYP for heme-NO models (other DFT functionals were applied to heme-NO models as well, results in Table S1). The standard 6-31G* basis set was used for all the atoms except Fe, on which Ahlrichs' valence triple-ζ (VTZ)[13, 14] basis set was employed. Calculations of geometry optimization and frequencies were performed with the Gaussian 03 program[15] applied with tight convergence criteria and an ultrafine integration grid.

All the frequency values were taken directly from the Gaussian program without scaling. Normal mode and isotopic shift analysis were performed by the TX90[16] program based on cartesian force constants calculated at the optimized geometry.

Results and Discussion

Raman spectra of 6-c NO and CO adducts

A principal objective of this work was to investigate the extent of backbonding in 6-coordinate (6-c) Fe(II)NO porphyrin adducts from the νFeN and νNO frequencies. RR spectra have been reported for such adducts only in heme proteins. Without the protein constraints, the *trans* axial ligand is too labile to permit acquisition of RR spectra in fluid solution. In our experience, even when sufficient ligand is added to assure complete formation of the 6-c adduct, as judged by the UV/VIS absorption spectrum, the RR spectrum is that of the 5-c adduct. Indeed, published reports of RR spectra of 6-c adducts have frequencies which are characteristic of 5-c adducts.[17,18] We infer that the Raman laser induces dissociation of the weak Fe-ligand bond, either photolytically or via local heating.

To overcome these problems, we resorted to freezing the sample, hoping that the frozen solvent matrix would induce rapid and efficient recombination of photo-dissociated ligand. This strategy succeeded, as illustrated in Figure 1. The RR spectrum of a frozen solution of (N-MeIm)Fe(II)T(2,6-F_2P)P(NO) in methylene chloride, to which ~9 M (final concentration) N-methylimidazole (N-MeIm) had been added, clearly showed νFeN and νNO bands at frequencies in the range of values seen for Fe(II)NO adducts of heme proteins, and very different from the values seen for 5-c adducts. The 1632 cm^{-1} νNO band is a shoulder on the side of a stronger porphyrin band, but the latter is subtracted out in the ^{14}NO-^{15}NO difference spectrum, which reveals the expected 32 cm^{-1} isotope shift. The 574 cm^{-1} νFeN band is more prominent, but is in a crowded region of the spectrum. The ^{14}NO-^{15}NO difference spectrum reveals a double band in the ^{15}NO spectrum, indicating that the νFeN mode has shifted into sufficiently close coincidence with a porphyrin mode to produce a Fermi resonance, in which intensity is shared between the two modes. Fermi resonances were previously encountered for the νNO RR band of 6-c Fe(II)NO adducts of Mb variants,[9] whose higher νNO frequency falls in another crowded region of porphyrin modes. As in that case, we determined an effective mode frequency by curve fitting the pair of RR difference bands, and averaging their

frequencies. The resulting frequency for the ^{15}NO isotopomer, gave the expected ~20 cm^{-1} isotope shift.

As in the previous 5-c adduct study,[2] we varied the extent of backdonation in a series of tetraphenylporphine adducts, having phenyl substituents, Y, with a range of electron donating or accepting properties. The isotope difference spectra are shown in Figure 2, and the frequencies are collected in Table 1. The νNO frequency increases systematically from the most (*p*-OCH_3P) to the least (F_5P) electron-donating phenyl substituent, while νFeN decreases in the same series. This pattern is the expected signature of backbonding.

Since protein-free 6-c Fe(II)CO adducts have not previously been studied systematically, we measured their RR spectra (Figures 3 and 4) as the phenyl-Y substituents were varied. Fewer representatives were available, since the electron withdrawing substituents tended to increase the photolability of CO, making acquisition of RR spectra difficult. Nevertheless, four pairs of νCO/νFeC frequencies (Table 1) were obtained, sufficient to establish the backbonding correlation (see next section).

TPP-X backbonding correlations

Figure 5 shows νFeX/νXO plots for 5- and 6-c Fe(II)porphyrin adducts with CO and NO. There is a remarkable parallelism, despite the different electronic structures of NO and CO. The νCO and νNO values are, of course, very different, reflecting the extra antibonding electron on NO, but the νFeC and νFeN values are similar, as is the range of variation in both sets of frequencies that are induced by the differing phenyl-Y substituents.

Negative correlations are obtained for all four sets of data, reflecting Fe-XO backbonding. As noted earlier[2] the slopes of the 5-c adduct plots are nearly the same for CO (-0.46) and NO (-0.40). The slope increases for the 6-c adducts, reflecting an increased sensitivity of νFeX for a given backbonding increment in νXO.[3] The increase is even larger for NO (-1.0) than for CO (-0.68). Thus, the sensitivity for νFeN is especially high, despite the impression gained from a set of myoglobin variants that the range of νFeN is small (see below).

The main difference between the CO and NO plots is that the 6-c line lies below the 5-c line for CO but above the 5-c line for NO. Adding an axial ligand depresses the νFeC frequency but elevates the νFeN frequency. There are two contributing factors to this difference, as discussed in the following section:

- **i.** The axial ligand lengthens the Fe-X bond for both Fe-C and Fe-N, but less so for Fe-N, due to the strong NO *trans* effect.
- **ii.** Because the Fe-N-O angle is bent, the Fe-N stretching coordinate mixes with the Fe-N-O bending coordinate, and this mixing increases when an axial ligand is bound.

The backbonding correlations can be cast in a standard form,[3] for ease of comparison: $\nu FeX = \nu°FeX - s[\nu XO - \nu°XO]$

where ν°XO is the frequency for unbound (gas phase) CO (2145 cm^{-1}) and NO (1876 cm^{-1}), and ν°FeX is the limiting (single-bond) frequency in the absence of backbonding. The parameters are collected in Table 2, where it can be seen that the ν°FeX limit values are quite similar for 5-c adducts, and are greatly depressed in both cases by the addition of axial ligand. The 6-c νFeN elevation seen for the actual NO complexes disappears for the limit value, because of the large 6-c slope. The limit values are, of course, entirely artificial, since backbonding is integral to the FeXO electronic structures.

DFT computation of structure

Our DFT-computed structures agree well with experimental data (Table 3 and Figure 6). For the NO adducts the bonds to the porphyrin N atoms are correctly predicted to be shorter in the direction of Fe-N-O bending. (This point is discussed in the crystal structure papers,[20,21] although the individual distances have been averaged in the reported distances – Table 3.)

The structures reveal the different responses of the CO and NO adducts to the addition of an imidazole ligand. In each case the Fe-X bond is lengthened, but the displacement is twice as large for CO (0.06 Å) as for NO (0.03 Å); theory and experiment agree on these displacements. In contrast, the Fe-ImH bond is longer for NO (2.24 Å) than for CO (2.08 Å): this is the well-known NO *trans* effect. Because the bond is weak, experimental bond distances for the bond *trans* to NO are somewhat variable, and Scheidt has not given a 'canonical' distance.[21] The computed Fe-ImH distance is close to that reported for the Fe-pyridine distance in (Py)Fe(TpivPP)(NO) (2.26 Å)[21] and somewhat longer than the Fe-N-methylimidazole distance in (N-MeIm)Fe(TPP)(NO) (2.17 Å). [21] For the CO adduct the computed Fe-ImH distance is close to experimental value for (N-MeIm)Fe(TPP)(CO) (2.05 Å),[22] and is somewhat longer than the 2.00 Å distance reported for the bis-imidazole adduct.[21]

The picture that emerges is that the *trans* ligand competes for bonding to Fe with either CO or NO. In both cases, the Fe-ImH and Fe-X bonds are both longer than if the opposite ligand is absent. However, the competition is fairly even for CO (~0.06 Å bond extension for both Fe-CO and Fe-ImH), but decidedly uneven for NO (0.03 Å extension for Fe-NO and 0.16 Å for Fe-ImH).

For the CO adducts, the widely used hybrid functional B3LYP serves very well, but we found that it gave poor results for the NO adducts. In particular, the calculation fails to capture the NO *trans* effect, as reported earlier.[2] The computed Fe-NO extension on binding ImH is too large, and the Fe-ImH bond is too short (Table S1 in supporting material). This deficiency can be traced to spin contamination (a problem also noted by Sage and coworkers[25]), due to low-lying high-spin excited states for the NO adducts[26] (but not for the CO adducts). The computed value of S^2 is 0.84 using B3LYP, and even higher for other hybrid functionals (Table S1) whereas, the expected value for one unpaired electron is 0.75. In contrast, non-hybrid functionals all gave $S^2 = 0.77$. Among those tried (Table S1), BLYP gave the best agreement with experimental structure parameters, and also with vibrational frequencies (next section). (However, we note that Negrerie et al[27] obtained somewhat different BLYP-computed FeP(NO) bond distances than those reported here, apparently because of a different basis set.) The spin contamination problem is due to the known tendency of hybrid functionals to exaggerate the stability of high-spin states.[28] This problem is discussed by Ghosh[29] in the context of iron porphyrins.

DFT-computed spectra and backbonding correlations

Vibrational modes were computed via DFT, and salient results are listed in Table 4. Discrepancies between experimental and DFT-computed frequencies are often adjusted by applying scale factors to various classes of vibrational coordinates.[30] Standard values are available for bonds in organic molecules, but not for metal-ligand bonds. The frequencies in Table 4 are unscaled, and show substantial deviations from experimental values, but the overall pattern is nevertheless instructive.

For the CO adducts, νCO is overestimated by ~150 cm^{-1}, while νFeC is overestimated for the 5-c adduct (by 35 cm^{-1}) but underestimated for the 6-c adduct (by 20 cm^{-1}). A substantial decrease in νFeC on binding ImH to the 5-c adduct is observed and computed, consistent with the Fe-C bond lengthening; simultaneously νCO increases slightly (observed and computed),

consistent with a very small (0.002 Å) shortening of the CO bond (Table 3). There is also a Fe-C-O bending mode, computed at 509 and ~570 cm^{-1} for the 5-c and 6-c adducts (there are two slightly different values for the 6-c adduct, corresponding to bending in and out of the plane defined by the ImH ligand). This mode is not normally enhanced in RR spectra for reasons of symmetry, but it has been detected in some heme protein CO adducts (where the symmetry can be lowered by steric or electrostatic forces) at ~570 cm^{-1},[31] in exact agreement with the computed 6-c value.

Symmetry also prevents mixing of the Fe-X stretching and Fe-X-O bending coordinates when the Fe-X-O unit is linear, as it is in the CO adducts. The potential energy entries in Table 4 confirm that the νFeC mode is essentially pure Fe-C stretching. However, the Fe-C-O bending contribution to δFeCO is only 50-65 %, because of mixing with the Fe-C tilting coordinate.[32]

When the Fe-X-O unit is bent, there is mixing between Fe-X stretching and Fe-X-O bending coordinates, producing two modes of mixed composition; the mixing also drives the mode frequencies apart. This phenomenon has been analyzed with empirical force fields in the context of protein-induced distortions of the Fe-C-O unit,[33] and the natural bending of the Fe-N-O unit.[34] Does this mixing vitiate the labeling of one of these modes as 'νFeN'? Table 4 indicates that the ~600 cm^{-1} mode, observed at 524 and 582 cm^{-1} in 5-c and 6-c NO adduct and identified via its large ^{15}NO shift, is indeed νFeN. The Fe-N stretching contribution is 95 % for the 5-c adduct and 66 % for the 6-c adduct. The mode having the highest Fe-N-O bending contribution is computed to be at 424 and 471 cm^{-1} for 5-c and 6-c adducts, and to have a small (3 cm^{-1}) ^{15}NO shift. The eigenvectors for these modes are shown in Fig. 7.

Praneeth[18] et al identified bands at 371 and 444 cm^{-1} in IR spectra of FeTPP(NO) and (N-MeIm)FeTPP(NO) as $^{15}N^{18}O$-sensitive. They assigned the first of these to δFeNO, but the second to νFeN, based on a 'quantum-chemistry-centered normal-coordinate analysis', in which selected force constants initially computed via DFT are refined empirically to fit the spectral data. They found the predominant contribution to be Fe-N stretching for the 444 cm^{-1} mode, and Fe-N-O bending for a 530 cm^{-1} mode, which they identified in the RR spectrum of (N-MeIm)FeTPP(NO). However, 530 cm^{-1} is the isotope-sensitive RR band for 5-c FeTPP (NO); in (N-MeIm)FeTPP(NO), the band shifts up to 582 cm^{-1} (Table 1). We infer that the RR laser induced ligand dissociation in the Praneeth et al's sample, even though it was contained in a KBr pellet. Consequently, the force constant refinement, and therefore the potential energy distribution, cannot have been correct.

Sage and coworkers[10] also proposed reassigning the 556 cm^{-1} mode in MbNO (the frequency is lower than in the protein-free 6-c adducts, as discussed below) from νFeN to δFeNO, since its NRVS band has a smaller Fe displacement than does another the NRVS band at 451 cm^{-1}. In addition NRVS on an oriented crystal of (N-MeIm)FeTPP(NO) revealed significant Fe motion perpendicular to the porphyrin plane for the lower frequency 440 cm^{-1} mode, but not for the higher frequency 540 cm^{-1} mode. Qualitatively, these observations are not inconsistent with our computed mode compositions. The eigenvectors (Figure 7) shows a larger Fe displacement (including the out-of-plane component) for the 472 cm^{-1} than the 601 cm^{-1} band, consistent with a larger computed $^{54/57}$Fe isotope shift for the former (Table 4).

However, the mode compositions in Table 4 may not be entirely correct, since there are discrepancies between the computed and experimental frequencies. A point of particular interest is the difficulty in reproducing the frequency upshift of νFeN, from 524 to 582 cm^{-1} upon binding N-MeIm to νFeN. As pointed out by Sage,[10] a decrease in νFeN might have been expected because of the ligand competition, and indeed the Fe-N bond distance does lengthen, as noted above, though not by as much as does the Fe-C distance in the CO adduct (0.03 vs 0.06 Å). Consistent with this lengthening the Fe-N force constant diminishes (3.61

mdyn/Å in FeP(NO) vs 3.21 mdyn/Å in (ImH)FeP(NO)), although again, not by as much as does the Fe-C force constant (3.51 mdyn/Å in FeP(CO) vs 2.44 mdyn/Å in (ImH)FeP(CO)). Countering the reduction in force constant, however, is a reduction in effective mass, from 17.9 amu for the 599 cm^{-1} mode of FeP(NO) to 14.7 amu for the 602 cm^{-1} mode of (ImH)FeP (NO), as a result of the νFeN/δFeNO coordinate mixing. The mode frequency does go up, but the 3 cm^{-1} computed elevation is far less than the 58 cm^{-1} observed elevation. Thus, the effective mass is still overestimated, suggesting that coordinate mixing would be greater if the mode were properly calculated.

In the face of this uncertainty about the exact mode composition, we propose to be pragmatic, and to simply assign 'νFeN' to the mode near 600 cm^{-1} that experiences a 15-20 cm^{-1} $^{14/15}N$ isotope shift (Table 1 and 4). This is the mode that shows a very good backbonding correlation, experimentally. (Whether the ~ 450 cm^{-1} mode also correlates with νNO is uncertain, since this band is very weak in the RR spectra of the NO adducts.)

We also examined the backbonding correlations computationally, by attaching electron withdrawing or donating substituents, Y, to the porphine ring, at either the pyrrole ring C_β outer atoms, or at the C_m atoms that bridge the pyrrole rings. The CO adducts gave quite good backbonding correlations (Figure 8), with slopes that were gratifyingly close to the experimental values (Table 2) for both 5- and 6-c adducts. (These slopes are considerably improved from those reported in a previous study,[2] due to the use of a larger basis set, VTZ instead of VDZ). Similar calculations for the NO adducts were less successful (Figure 8). The 6-c adducts did correlate linearly, but the slope was much lower than the experimental slope (Table 2), while the 5-c adducts showed a weak correlation, with considerable scatter.

Thus the backbonding correlations are satisfactorily modeled for CO but not NO by employing substituents directly attached to the porphyrin ring. The experimental data are for substituents located on the phenyl group of TPP, at one remove from the porphyrin itself. The effect of this difference can not be evaluated computationally because the TPP-Y adduct have too many atoms for practicable DFT calculations with a series of substituents.

We speculate that the unsatisfactory modeling of the NO correlations stems from the complex orbital structure of the NO adducts, illustrated in Figure 9 (and discussed more fully in Ghosh's studies[35]). In the two highest occupied orbitals, the NO antibonding π* orbital in the bending plane (xz) interact strongly with the d_{z^2} orbital on the one hand and the d_{xz} orbital on the other. The third HOMO involves a classical backbonding interaction, between the out-of-plane π* orbital and d_{yz}. In the CO adducts, the two highest orbitals are both of this backbonding character, while the third involves porphyrin orbitals only (Figure S1). Thus the backbonding correlations for CO adducts result from a straightforward d_π-π* interaction, which is influenced by inductive substituent effects. For NO adducts however, the complex interplay between d_{xz} and d_{z^2} may be influenced by the porphyrin π orbitals (which are no longer orthogonal to d_{z^2} because of its tilt (Figure 9)), and this influence may vary for different substituents when they are directly on the ring. We note that similar complexities were found by Rodgers and coworkers in computing backbonding correlations for Fe(III)NO adducts.[36]

Protein effects and the FeXO angle

In Figure 10 we plot νFeX/νXO data from the literature for both CO and NO adducts of several heme proteins (see Table 5). The lines are those obtained experimentally from the protein-free TPP-Y porphyrins (Figure 5). The 6-c protein-free CO line describes the protein-CO adducts quite well, as expected from many previous studies.[4] There are certain, well-understood exceptions. Thus cytochrome P450 falls below the line because imidazole is replaced as axial ligand by thiolate, a stronger donor, which further weakens the Fe-CO bond. On the other hand, the positive deviation for cytochrome oxidase is believed to result from compression of the Fe-

CO bond by a Cu^+ ion, which lies close to the distal end of the bound CO in the binuclear heme-Cu site.[4] The remaining proteins fall close to the line at positions that reflect the backbonding influence of distal groups. Thus, wild-type myoglobin (WT Mb) lies high on the line (low νCO, high νFeC) thanks to the polar effect of the distal histidine (H64), which donates a weak H-bond to the bound CO, enhancing the extent of backbonding. For the Mb variants H64L and H64I, in which the distal histidine is replaced by the hydrophobic residues leucine and isoleucine, this effect is absent, and the points shift down the backbonding line. Other proteins represented in Figure 10, principally representing heme sensor proteins, cluster in the same region, and presumably have hydrophobic binding pockets.

The NO data is more scattered, but the hydrophobic Mb variants and the heme sensor proteins nevertheless fall close to the 6-c protein-free line. Thus 6-c NO adducts are not necessarily different in a protein than outside a protein. Cytochrome P450 falls well below the line, as it does for the CO adducts, and presumably for the same reason, that the axial ligand is thiolate, a strong donor.

However, there are striking deviations from the 6-c protein-free line for some NO adducts, even though the axial ligand remains imidazole. One of these is WT Mb, which falls far below the line. Similarly positioned are neuroglobin and cytoglobin; these share with WT Mb the presence of a distal histidine residue.[43] Also anomalous is cytochrome oxidase. The distal Cu^+ ion which displaces the CO adduct *above* the 6-c CO line, presumably because of a compressive effect, instead displaces the NO adduct *below* the 6-c NO line, to a position close to WT Mb. The common feature of all four deviant points is the presence of a positively polar entity, histidine or Cu^+, on the distal side of the bound NO.

We considered the possibility that negative deviations from the 6-c NO adduct correlation might result from weakening or breaking of the axial imidazole bond, thereby moving the point toward the 5-c line (Figure 10). This bond is weak and is easily stretched[2, 46] and broken. For example, lowering the pH of MbNO to 4 is sufficient to break the bond protonate the proximal histidine.[47] However, there is no reason to link axial bond weakening with distal positive polarity. This issue has been checked computationally by Tangen et al,[11c] who found that the axial imidazole bond is actually strengthened by distal H-bond donors.

Earlier we suggested[9] that the anomalous νFeN/νNO values in WT Mb might result from further reduction of the FeNO angle from its unconstrained value, induced by steric and/or electrostatic interaction with the distal histidine sidechain. Trial DFT calculations, using B3LYP, produced large reductions in both νFeN and νNO when the FeNO angle was constrained to be 10° smaller than its computed equilibrium value, 142°. We repeated this calculation using BLYP, which gives a better account of the ground state structure, as discussed above, and obtained essentially the same result (Table 6). Reducing the FeNO angle by 10°, from the equilibrium value of 139°, reduced νFeN by 26 cm^{-1}, and νNO by 35 cm^{-1} (the previous calculation predicted 41 an 74 cm^{-1} reductions[9]). In contrast, increasing the FeNO angle by 10° produced a smaller νNO increase (28 cm^{-1}) and essentially no change in νFeN. The difference reflects both electronic and kinematic effects, as discussed previously.[9] Reducing the FeNO angle lengthens the Fe-NO bond and contracts the Fe-ImH bond slightly, while increasing the angle has the opposite effect (Table 6). These trends are consistent with expected changes in resonance structure (Figure 11). Opening the angle favors the linear Fe(I)(NO^+) structure, in which the NO is triple-bonded. Its antibonding electron is transferred to the Fe d_z2 orbital, lengthening the Fe-ImH bond. Closing the angle favors the Fe(III)(NO^-) structure, in which two electrons occupy the NO π* orbital, producing double-bonded NO^-, and the d_z2 orbital is emptied, shortening the Fe-ImH bond. The energies required to increase or decrease the FeNO angle by 10° are small, 1.4 and 1.2 kcal/mol, reflecting the electronic flexibility of the FeNO system. We note that the observed differences between WT Mb, and

the H64L variant, which lies near the 6-c adduct line, are 11 cm^{-1} for νFeN and 23 cm^{-1} for νNO, roughly half the predicted effects for a 10° closing of the FeNO angle. Thus, small angle changes can produce the large observed deviations from the backbonding correlation.

Structural data on the FeNO angle in MbNO are ambiguous. There are two published X-ray crystal structures of MbNO, one of which found a surprisingly acute angle, 112°,[48] while the other found a normal angle, 147°,[49] as did a frozen solution EXAFS study.[46] The two crystal structures were both at medium resolution, 1.7 and 1.9 Å, and the discrepancy between them is a puzzle, especially as there seems to be no significant difference in the disposition of the distal histidine, or of other distal groups. In both crystallographic studies, the samples were prepared by nitrosylation of aquo-metMb crystals, so it is conceivable that sample history somehow influenced the structures. Reinforcing this possibility is early EPR evidence indicating large changes in the FeNO angle with temperature.[51,52]

In any event, the vibrational data support the hypothesis that properly oriented distal groups with positive polarity can produce modest closure of the FeNO angle, with large effects on νFeN and νNO. If this new angle were held constant, then a new backbonding correlation would presumably apply. We checked this expectation by recalculating frequencies for the 6-c (ImH) FeP-Y(NO) series with the FeNO angle constrained to be 129°; the resulting data describe a backbonding line, which is shifted down but is parallel to the line for the equilibrium angle (Figure 8).

With these considerations in mind, we reexamined the data[9] on a series of Mb variants with specific residue replacements in the distal pocket (Figure 12 – see inset for the arrangement of distal groups.). The CO adducts all fall on the protein-free 6-c backbonding correlation, at positions reflecting the control of backbonding by electrostatic effects. As mentioned above, hydrophobic replacements of His64 produce points at the low end of the line, due the loss of H-bonding. However, the H64Q replacement moves the point only part way down the line, since the glutamine sidechain retains some H-bond donor ability. At the same time, introduction of a bulky phenylalanine sidechain for Leu29, at the back of the pocket reinforces the H-bond, either from histidine (L29F variant) or from glutamine (L29F/H64Q variant), moving both points up the line. On the other hand the orientation of His64 in WT Mb is maintained by the phenyl ring of Phe46, and its replacement by valine allows the His64 sidechain to move away from the CO, leaving a hydrophobic environment;[53, 54] the point for F46V is at the bottom of the line. Finally substitution of asparagine for Val68, which is in direct contact with the bound CO (and is responsible for the small (8°) deviation from FeCO linearity[55]) introduces a strong H-bond; V68N is at the top of the line. Thus, the strength of the H-bond interaction is directly reflected by the νFeC/νCO position on the backbonding correlation.

This is definitely not the pattern seen for NO adducts of the same variants, for which we notice instead that the distal H-bonds induce a displacement *from* the 6-c NO line which increases with the magnitude of the interaction. The largest displacement is seen for V68N, which shows the largest backbonding augmentation for the CO adduct. The substantial displacement of WT Mb is increased when Leu29 is substituted by phenylalanine, augmenting the His 64 H-bond. On the other hand, the displacement is diminished when His64 is replaced by glutamine, the weaker H-bonder, and essentially disappears for the H64L and H64I hydrophobic replacements. Likewise, the WT displacement diminishes successively when the buttressing effect of Phe46 is relaxed by replacement with smaller sidechains from leucine, valine or alanine.

This pattern suggests that the distal H-bonds close down the FeNO angle and that the stronger the interaction the smaller the angle. As seen from our model calculations, the extent of angle change need not be large to produce the observed frequency changes, but the direction of the

effect is clear. At the same time, however, H-bonding is also expected to increase νFeN while decreasing νNO by increasing the backbonding interaction, just as in the CO adducts. This can explain why most of the observed displacements from the line mainly involve νNO, with little variation in νFeN. (The small νFeN variation is what led Boxer to infer that backbonding is unimportant in NO adducts.[8]) If H-bonding decreases the FeNO angle, the accompanying increase in backbonding would reinforce the angle-induced diminution of νNO, but would counteract it in the case of νFeN, producing the observed horizontal spread for most of the points.

However, some of the variants show appreciable changes in νFeN, suggesting backbonding changes independent of angle changes. Intriguingly the points for F46V, H64Q, L29F/H64Q and V68F are ranged along a line parallel to the 6-c protein free line. This is the behavior expected for variable backbonding at constant FeNO angle, as confirmed by our model calculations on (ImH)FeP-Y(NO) with constrained FeNO angle (Figure 8).

Why should H-bonding affect the FeNO angle? We suggest that the answer lies in the interaction of geometry with resonance structure, as mentioned above. Smaller angles are associated with the $Fe(III)NO^-$ resonance structure, and this structure should be favored by H-bond donors. However, the orientation of the H-bond donor is critical because the FeNO angle affects the charge differently on the N and O atoms. The DFT calculation (Table 6) shows negative charge increasing on N but decreasing on O as the FeNO angle decreases. The total charge on NO changes very little. This is because the formal charges in the resonance structures (Figure 11) are compensated by backbonding, which is greater for $Fe(I)NO^+$ (having two d_π-π^* interactions) than for $Fe(III)NO^-$ (having one d_π-π^* interaction). Thus increased FeNO bending would be favoured if a distal H-bond donor is oriented toward the N atom of the bound NO (Figure 11). This is in fact the orientation of the distal histidine in MbNO (Figure 12, inset). In contrast, a distal tyrosine H-bond donor in the TtTar4H domain points toward the O atom (judging from the crystal structure of the O_2 adduct[56]), and the νFeN/νNO point for this protein does fall on the 6-c adduct line (Figure 10). We have carried out preliminary DFT calculations, which support the idea that H-bond donors affect the FeNO angle if they point at the N, but not the O atom. This interaction also explains why the CO and NO adducts are so different in their vibrational responses to H-bond effects (Figure 11). H-bond donation simply polarizes the FeCO orbitals, without an inherent effect on the geometry. Because the FeCO unit lacks the antibonding electron that shifts back and forth in FeNO with changing angle, the FeCO geometry is indifferent to polarization. Conversely, modest changes in the FeCO angle, which can result from steric effects,[55] produce small changes in νFeC and νCO.[57]

These considerations suggest how the electronic flexibility of the FeNO unit adds a dimension of complexity to the interpretation of structure and spectra. The spread of points in both directions of the νFeN/νNO plots make NO a highly sensitive probe of protein influences, more so than CO. The data reflect not only the presence, but also the directionality of distal polar groups. It is possible that the N-specific H-bond effect also accounts for the altered rhombicity seen in temperature dependent EPR and ENDOR of various heme protein NO adducts, and characterized as type I and II.[58] A distal histidine signal has been tentatively identified in type II spectra,[59] which may be associated with H-bond anomalies seen in the νFeN/νNO vibrational data.

Conclusions

Although the bent FeNO structure of heme-NO adducts induces mixing of Fe-N stretching and Fe-N-O bending coordinates, a $^{15/14}$NO-sensitive vibrational band in the 500-600 cm^{-1} region can still be identified as ‘νFeN’. Plots of this frequency against νNO produce negative linear correlations for both 5- and 6-coordinate adducts of Fe(II)TPP-Y adducts with variably

electron-donating Y substituents, quite similar to νFeC/νCO correlations of the corresponding CO adducts.

However, CO and NO adducts respond very differently to protein influences, especially to distal H-bond donors or positive charges. While the νFeC/νCO points move up and down the backbonding correlation, in proportion to the strength of the polar interaction, the νFeN/νNO points deviate strongly from the correlation, in the same order of interaction strength. These deviations are judged to result from diminution of the FeNO angle due to the polar stabilization of the Fe(III)(NO^-) valence isomer, a stereoelectronic effect which is absent for CO adducts. This added effect may be useful in probing the determinants of ligand discrimination and signaling in heme proteins.

Supplementary Material

Refer to Web version on PubMed Central for supplementary material.

Acknowledgements

We thank Dr. Ingar Wasbotten and Dr. Andrzej Jarzecki for preliminary work on this project, and Prof. John Olson for helpful discussions. This work was supported by NIH grant GM 33576.

References

1. (a) Rodgers KR. Curr Opin Chem Biol 1999;3:158–67. [PubMed: 10226051] (b) Gilles-Gonzalez MA, Gonzalez G. J Inorg Biochem 2005;99:1–22. [PubMed: 15598487] (c) Boon EM, Marletta MA. Curr Opin Chem Biol 2005;9:441–446. [PubMed: 16125437] (d) Roberts GP, Kerby RL, Youn H, Conrad M. J Inorg Biochem 2005;99:280–292. [PubMed: 15598507]
2. Vogel KM, Kozlowski PM, Zgierski MZ, Spiro TG. J Am Chem Soc 1999;121:9915–9921.
3. Vogel KM, Kozlowski PM, Zgierski MZ, Spiro TG. Inorg Chimica Acta 2000;297:11–17.
4. Spiro TG, Wasbotten IH. J Inorg Biochem 2005;99:34–44. [PubMed: 15598489]
5. Coyle CM, Puranik M, Youn H, Nielsen SB, Williams RD, Kerby RL, Roberts GP, Spiro TG. J Biol Chem 2003;278:35384–35393. [PubMed: 12796503]
6. Ibrahim M, Kerby RL, Puranik M, Wasbotten IH, Youn H, Roberts GP, Spiro TG. J Biol Chem 2006;281:29165–29173. [PubMed: 16873369]
7. Thomas MR, Brown D, Franzen S, Boxer SG. Biochemistry 2001;40:15047–15056. [PubMed: 11732927]
8. Park ES, Boxer SG. J Phys Chem B 2002;106:5800–5806.
9. Coyle CM, Vogel KM, Rush TS III, Kozlowski PM, Williams R, Spiro TG, Dou Y, Ikeda-Saito M, Olson JS, Zgierski MZ. Biochemistry 2003;42:4896–4903. [PubMed: 12718530]
10. Zeng W, Silvernail NJ, Wharton DC, Georgiev GY, Leu BM, Scheidt WR, Zhao J, Sturhahn W, Alp EE, Sage JT. J Am Chem Soc 2005;127:11200–11201. [PubMed: 16089422]
11. (a) Zhang Y, Gossman W, Oldfield E. J Am Chem Soc 2003;125:16387–16396. [PubMed: 14692781] (b) Praneeth VKK, Neese F, Lehnert N. Inorg Chem 2005;44:2570–2572. [PubMed: 15819537] (c) Tangen E, Svadberg A, Ghosh A. Inorg Chem 2005;44:7802–7805. [PubMed: 16241129]
12. Stong JD, Burke JM, Daly P, Wright P, Spiro TG. J Am Chem Soc 1980;102:5815–5819.
13. Schafer A, Horn H, Ahlrichs R. J Chem Phys 1992;97:2571–2577.
14. Bauernschmitt R, Ahlrichs R. Chem Phys Lett 1996;256:454–464.
15. Frisch, MJ., et al. Gaussian 03. Gaussian, Inc.; Wallingford, CT: 2004.
16. Pulay, P. TX90. Fayetteville, AR: 1990. Pulay P. Theor Chim Acta 1979;50:299–312.
17. Lipscomb LA, Lee BS, Yu NT. Inorg Chem 1993;32:281–286.
18. Praneeth VKK, Nather C, Peters G, Lehnert N. Inorg Chem 2006;45:2795–2811. [PubMed: 16562937]
19. Song S, Boffi A, Chiancone E, Rousseau DL. Biochemistry 1993;32:6330–6336. [PubMed: 8518278]

20. Scheidt WR, Haller KJ, Fons M, Mashiko T, Reed CA. Biochemistry 1981;20:3653–3657. [PubMed: 7260062]
21. Wyllie GRA, Schulz CE, Scheidt WR. Inorg Chem 2003;42:5722–5734. [PubMed: 12950223]
22. Silvernail NJ, Roth A, Schulz CE, Noll BC, Scheidt WR. J Am Chem Soc 2005;127:14422–14433. [PubMed: 16218637]
23. Scheidt WR, Frisse ME. J Am Chem Soc 1975;97:17–21. [PubMed: 1133330]
24. Nasri H, Haller KJ, Wang Y, Hanh HB, Scheidt WR. Inorg Chem 1992;31:3459–3467.
25. Leu BM, Zgierski MZ, Wyllie GRA, Scheidt WR, Sturhahn W, Alp EE, Durbin SM, Sage JT. J Am Chem Soc 2004;126:4211–4227. [PubMed: 15053610]
26. Rovira C, Kunc K, Hutter J, Ballone P, Parrinello M. J Phys Chem A 1997;101:8914–8925.
27. Negrerie M, Kruglik SG, Lambry JC, Vos MH, Martin JL, Franzen S. J Biol Chem 2006;281:10389–10398. [PubMed: 16476730]
28. Reiher M, Salomon O, Hess BA. Theor Chem Acc 2001;107:48–55.
29. Ghosh A. J Biol Inorg Chem 2006;11:712–724. [PubMed: 16841211]
30. (a) Rauhut G, Pulay P. J Am Chem Soc 1995;117:4167–4172. (b) Rauhut G, Jarzecki AA, Pulay P. J Comput Chem 1997;18:489–500.
31. (a) Tsubaki M, Srivastava RB, Yu NT. Biochemistry 1982;21:1132–1140. [PubMed: 7074069] (b) Vogel KM, Spiro TG, Shelver D, Thorsteinsson MV, Roberts GP. Biochemistry 1999;38:2679–2687. [PubMed: 10052938] (c) Fan B, Gupta G, Danzier RS, Friedman J, Rouessau DL. Biochemistry 1998;37:1178–1184. [PubMed: 9477941] (d) Vogel KM, Hu S, Spiro TG, Dierks EA, Yu AE, Burstyn JN. J Biol Inorg Chem 1999;4:804–813. [PubMed: 10631613]
32. Ghosh A, Bocian DF. J Phys Chem 1996;100:6363–6367.
33. Li XY, Spiro TG. J Am Chem Soc 1988;110:6024–6033.
34. Hu SZ, Kincaid JR. J Am Chem Soc 1991;113:9760–9766.
35. Ghosh A. Acc Chem Res 2005;38:943–954. [PubMed: 16359166]
36. (a) Linder DP, Rodgers KR, Banister J, Wyllie GRA, Ellison MK, Scheidt WR. J Am Chem Soc 2004;126:14136–14148. [PubMed: 15506779] (b) Linder DP, Rodgers KR. Inorg Chem 2005;44:1367–1380. [PubMed: 15732977]
37. Andrew CR, George SJ, Lawson DM, Eady RR. Biochemistry 2002;41:2353–2360. [PubMed: 11841228]
38. Andrew CR, Kemper LJ, Busche TL, Tiwari AM, Kecskes MC, Stafford JM, Croft LC, Lu S, Möenne-Loccoz P, Huston W, Moir JWB, Eady RR. Biochemistry 2005;44:8664–8672. [PubMed: 15952773]
39. Tomita T, Gonzalez G, Chang AL, Ikeda-Saito M, Gilles-Gonzalez MA. Biochemistry 2002;41:4819–4826. [PubMed: 11939776]
40. Karow, David S.; Pan, D.; Tran, R.; Pellicena, P.; Presley, A.; Mathies, RA.; Marletta, MA. Biochemistry 2004;43:10203–10211. [PubMed: 15287748]
41. Pinakoulaki E, Ohta T, Soulimane T, Kitagawa T, Varotsis C. J Biol Chem 2004;279:22791–22794. [PubMed: 15066990]
42. Pinakoulaki E, Ohta T, Soulimane T, Kitagawa T, Varotsis C. J Am Chem Soc 2005;127:15161–15167. [PubMed: 16248657]
43. Sawai H, Makino M, Mizutani Y, Ohta T, Sugimoto H, Uno T, Kawada N, Yoshizato K, Kitagawa T, Shiro Y. Biochemistry 2005;44:13257–13265. [PubMed: 16201751]
44. Nagano S, Shimada H, Tarumi A, Hishiki T, Kimata-Ariga Y, Egawa T, Suematsu M, Park SY, Adachi S, Shiro Y, Ishimura Y. Biochemistry 2003;49:14507–14. [PubMed: 14661963]
45. Unno M, Christian JF, Sjodin T, Benson DE, Macdonald ID, Sligar SG, Champion PM. J Biol Chem 2002;277:2547–2553. [PubMed: 11706033]
46. (a) Maréchal J, Barea G, Maseras F, Lledós A, Mouawad L, Pérahia D. J Comput Chem 2000;21:282–294. (b) Patchkovskii S, Ziegler T. Inorg Chem 2000;39:5354–5364. [PubMed: 11154592]
47. Duprat AF, Traylor TG, Wu GZ, Coletta M, Sharma VS, Walda KN, Magde D. Biochemistry 1995;34:2634–2644. [PubMed: 7873545]
48. Brucker EA, Olson JS, Ikeda-Saito M, Phillips GN. Proteins 1998;30:352–356. [PubMed: 9533619]
49. Copeland DM, West AH, Richter-Addo GB. Proteins 2003;53:182–192. [PubMed: 14517970]

50. Rich AM, Armstrong RS, Ellis PJ, Lay PA. J Am Chem Soc 1998;120:10827–10836.
51. Chien JCW. J Chem Phys 1969;51:4220–4227. [PubMed: 4311919]
52. Hori H, Ikeda-Saito M, Yonetani T. J Biol Chem 1981;256:7849–7855. [PubMed: 6267028]
53. Li TS, Quillin ML, Phillips GN, Olson JS. Biochemistry 1994;33:1433–1446. [PubMed: 8312263]
54. Lai HH, Li TS, Lyons DS, Phillips GN, Olson JS, Gibson QH. Proteins 1995;22:322–339. [PubMed: 7479707]
55. De Angelis F, Jarzecki AA, Car R, Spiro TG. J Phys Chem B 2005;109:3065–3070. [PubMed: 16851321]
56. Pellicena P, Karow DS, Boon EM, Marletta MA, Kuriyan J. Proc Natl Acad Sci USA 2004;101:12854–12859. [PubMed: 15326296]
57. Kozlowski PM, Vogel KM, Zgierski MZ, Spiro TG. J Porphyrins Phthalocyanines 2001;5:312–322.
58. (a) Hüttermann J, Burgard C, Kappl R. J Chem Soc Faraday Trans 1994;90:3077–3087. (b) Flores M, Wajnberg E, Bemski G. Biophys J 1997;73:3225–3229. [PubMed: 9414233] (c) Hori H, Ikeda-Saito M, Yonetani T. J Biol Chem 1981;256:7849–7855. [PubMed: 6267028]
59. Tyryshkin AM, Dikanov SA, Reijerse EJ, Burgard C, Hüttermann J. J Am Chem Soc 1999;121:3396–3406.

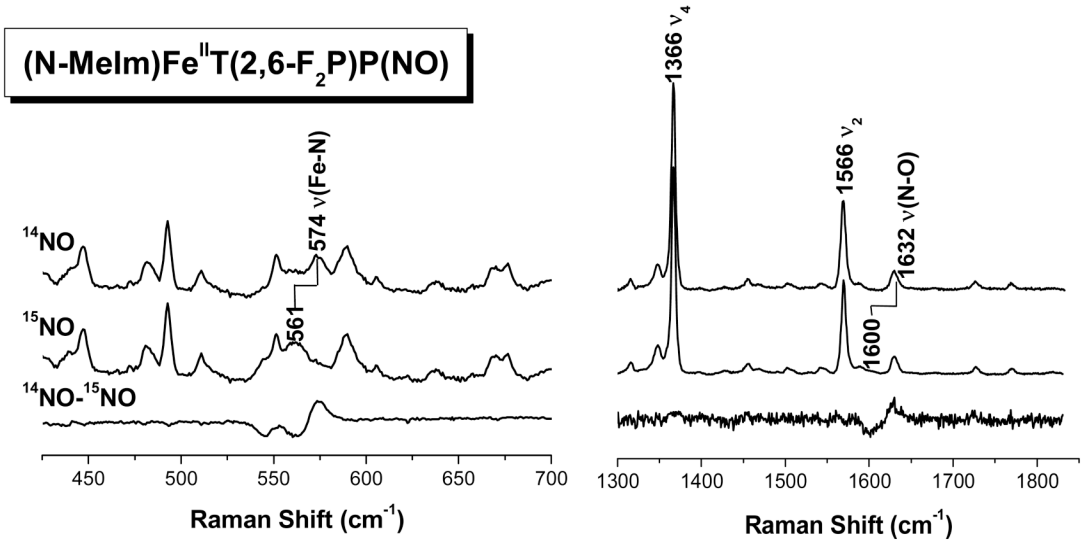

Figure 1.
RR spectra (413.1nm excitation) for frozen solutions (77K) of (N-MeIm)Fe(II)T(2,6-F_2P)P (NO) containing ^{14}NO or ^{15}NO, and the difference spectra.

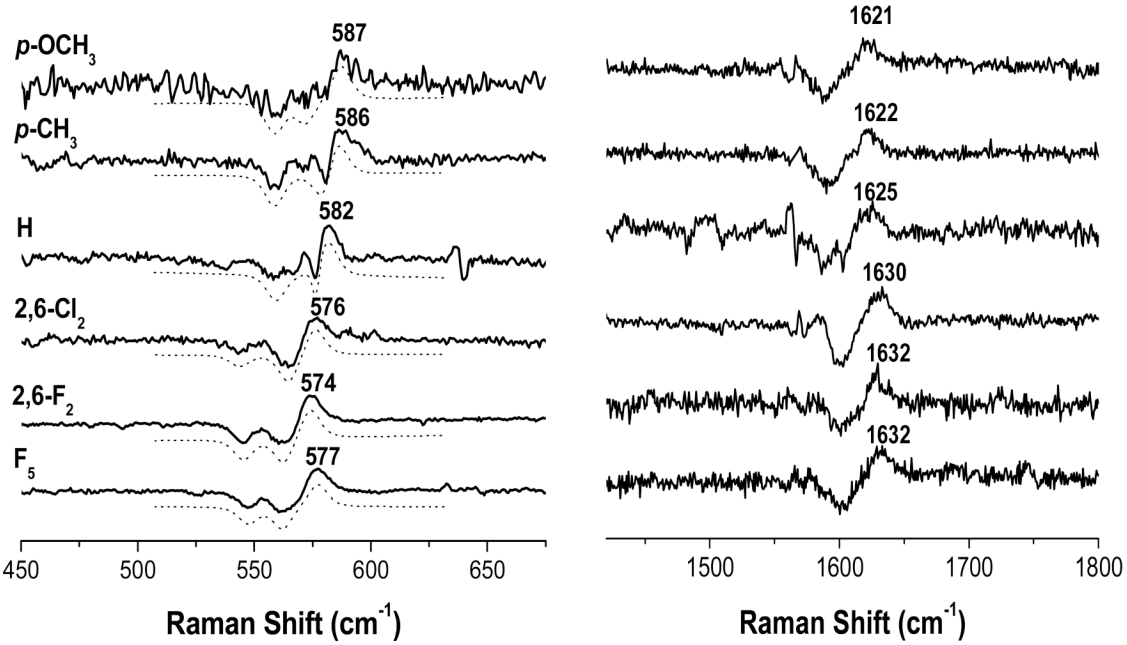

Figure 2.

RR difference spectra (^{14}NO - ^{15}NO) of (N-MeIm)Fe(II)(TPP-Y)(NO) with the indicated phenyl substituent, Y. The dotted lines are the results of curve fitting (50% Gaussian/ 50% Lorentzian, with 10cm^{-1} bandwidths) to resolve the ^{15}NO Fermi resonance at ~550 cm^{-1}.

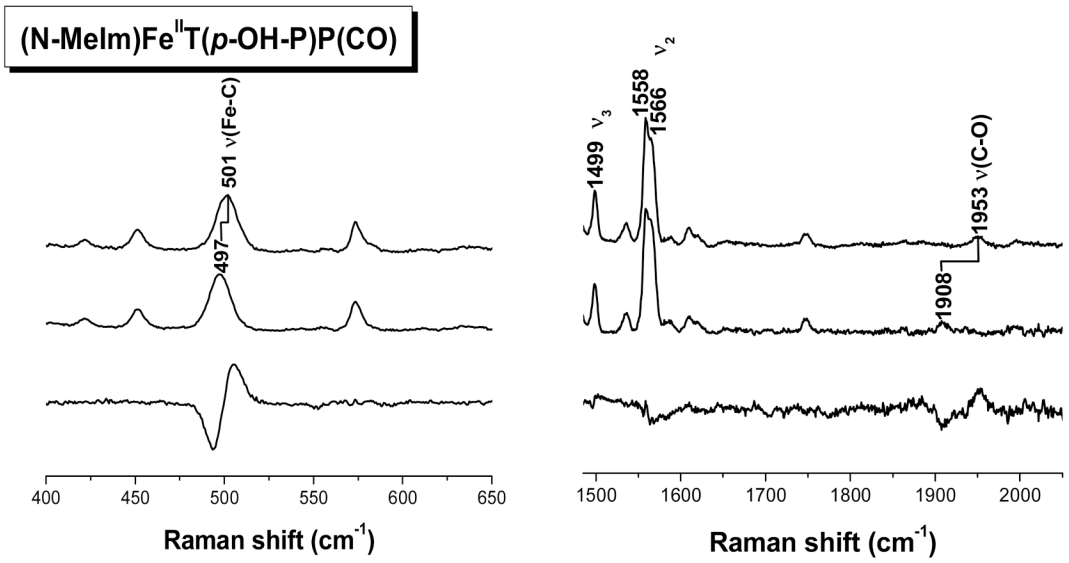

Figure 3.
RR spectra (413.1nm excitation) for frozen solutions (77K) of (N-MeIm)Fe(II)T(*p*-OH-P)P(CO) containing ^{12}CO or ^{13}CO, and the difference spectra.

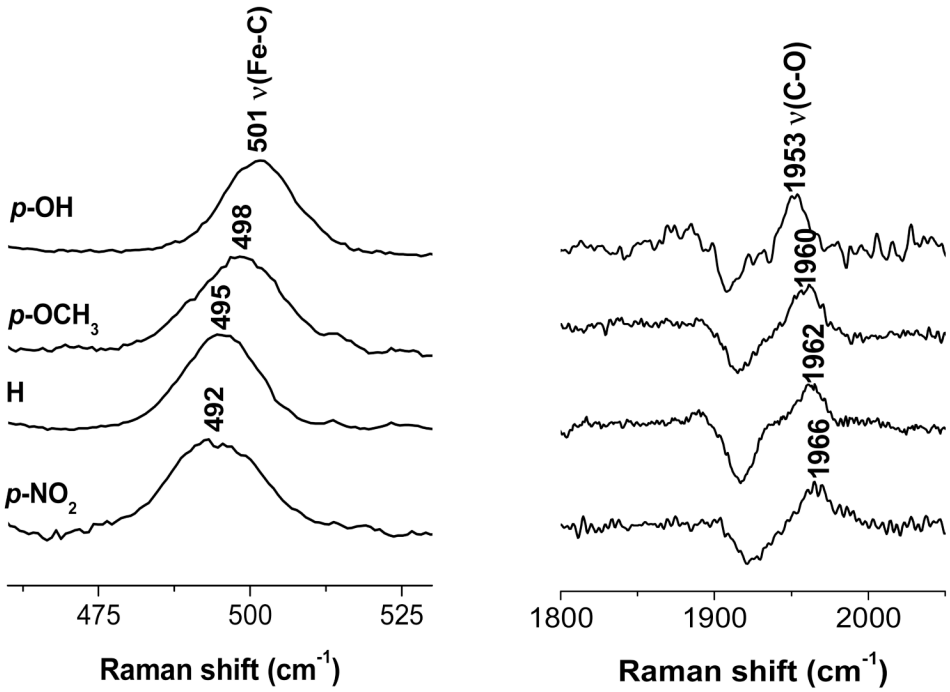

Figure 4.

RR spectra (low frequency region, left) and difference spectra ($^{12}CO - ^{13}CO$) (high-frequency region, right) of (N-MeIm)Fe(II)(TPP-Y)(CO) with the indicated phenyl substituent, Y. (The Fe-C band itself is shown instead of the isotope difference band, whose positive and negative lobes do not accurately represent mode frequencies in this case because of the small isotope shift (ref [19]).

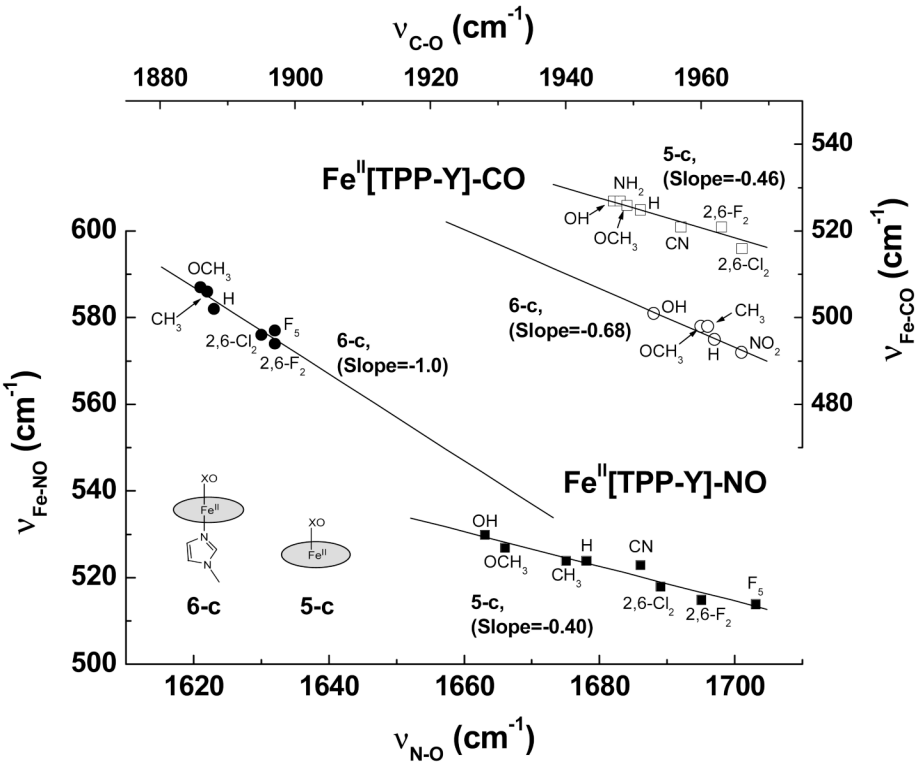

Figure 5.

FeXO backbonding correlations for 5-c and 6-c (N-MeIm axial ligand) NO and CO adducts of Fe(II)TPP-Y with the indicated phenyl substituents, Y, in organic solvents (CH_2Cl_2, DMF, Bz). For the 5-c adducts NO data are from [ref [2]], and CO data are from [ref [3]]. The 6-c adduct data are from Table 1.

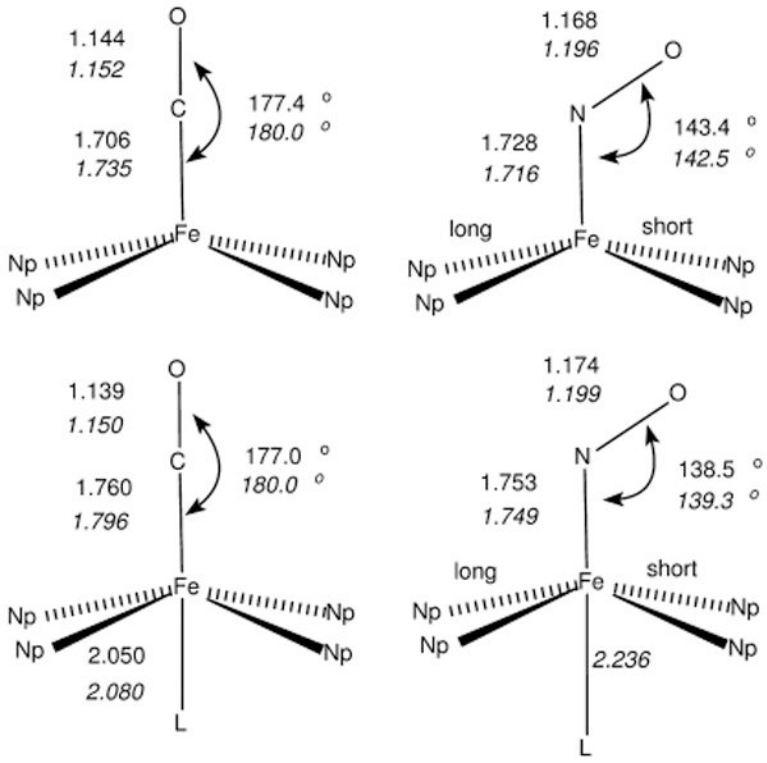

Figure 6.

Geometry comparison between experimental[a] and computational (italics) results of Fe(II)P(XO) and (ImH)Fe(II)P(XO)

[a] See Table 3; Scheidt's 'canonical' values are used for Fe(II)NO adducts.

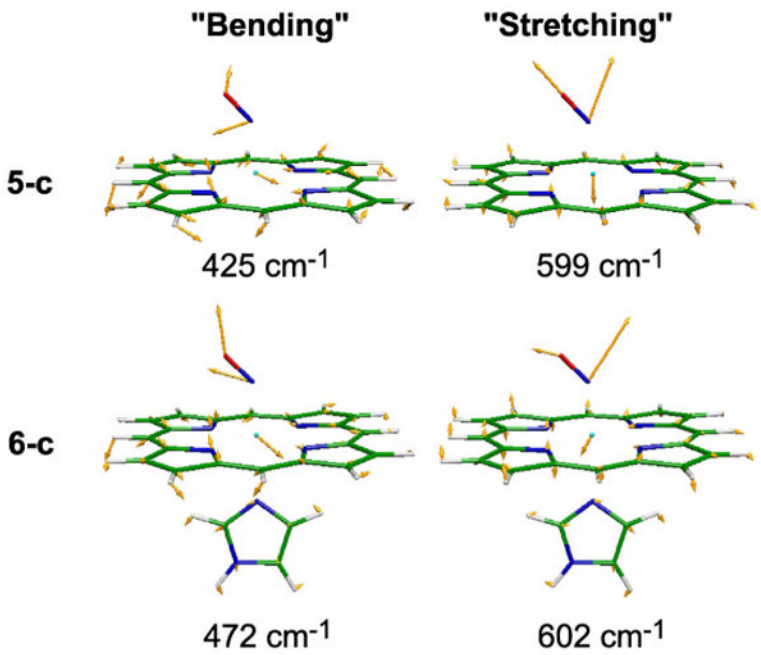

Figure 7.
Eigenvectors of Fe(II)NO “bending” and “stretching” modes (computed frequencies). The stretching and bending internal coordinates are substantially mixed (see discussion).

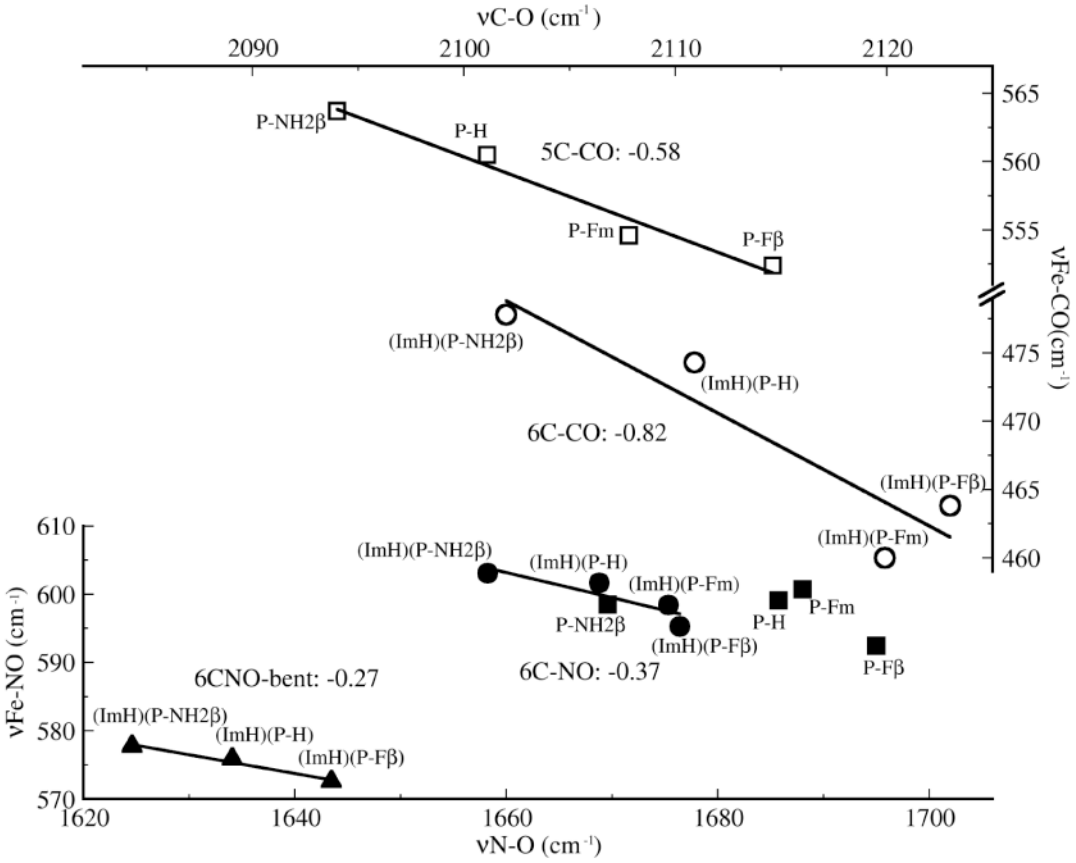

Figure 8.

νFeX/νXO anti-correlation computed via DFT (B3LYP for CO, BLYP for NO) for FeP-Y(XO) (□ CO, ■ NO) and (ImH)FeP-Y(XO) (○ CO, ● NO); the Y substituents and its attachment to C_β or C_m atoms of the porphine are indicated. Lines are drawn with the indicated least-squares slopes. "Bent" refers to (ImH)FeP-Y(NO) (labeled as ▲) calculations in which the FeNO angle was constrained at 129°.

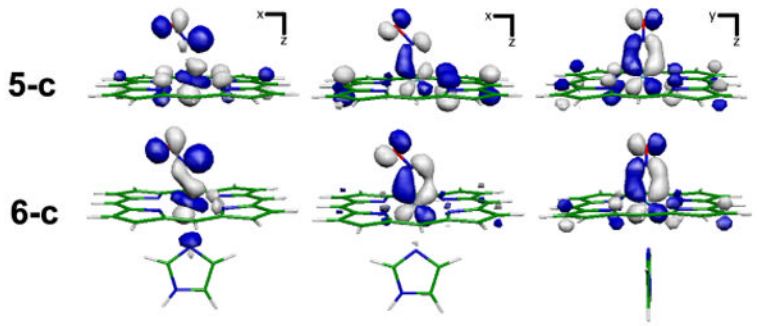

Figure 9.
Three highest HOMOs with major contribution from the FeNO moiety of Fe(II)P(NO) and (ImH)Fe(II)P(NO).

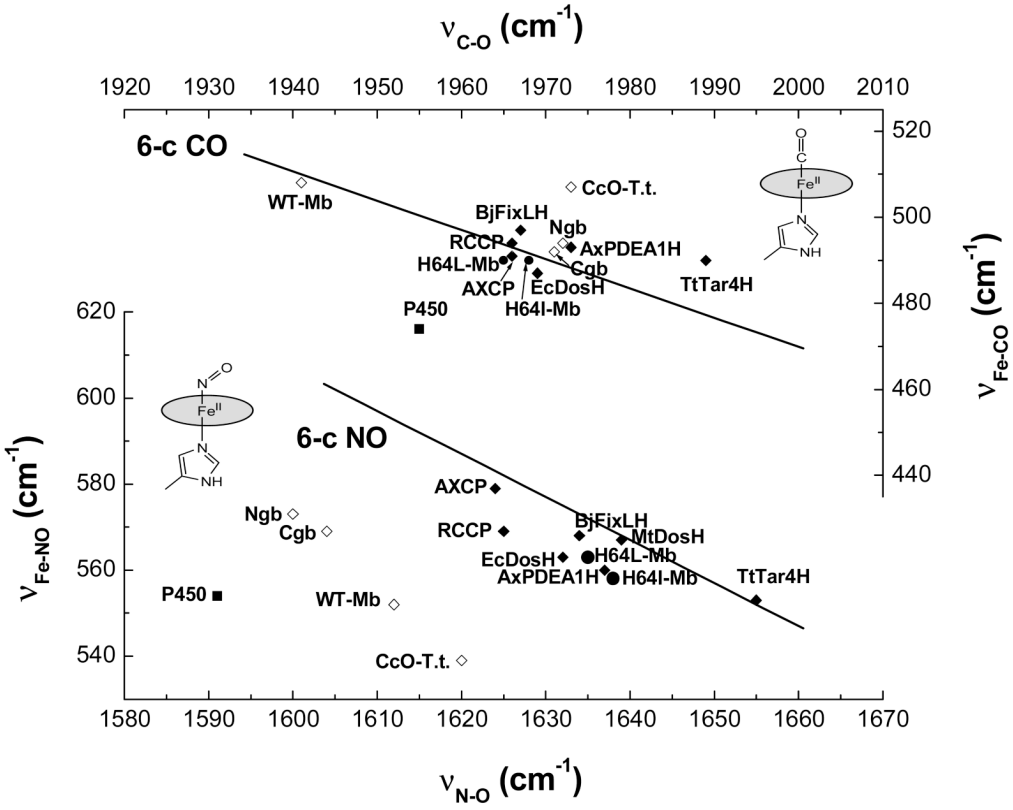

Figure 10.

vFeX/vXO plot for available data from heme protein Fe(II)XO adducts (see Table 5). The filled circles are H64L and H64I variants of Mb. Open diamonds are proteins with distal histidine (Ngb, Cgb and WT-Mb) or, in the case of CcO, with a distal Cu_B center. The filled square is a cyt $P450_{cam}$ bound adamantanone. Cytchrome P450 has a cysteine axial ligand; the other proteins all have histidine ligands. The backbonding correlations (solid lines) are for 6-c protein free adducts (from Figure 5).

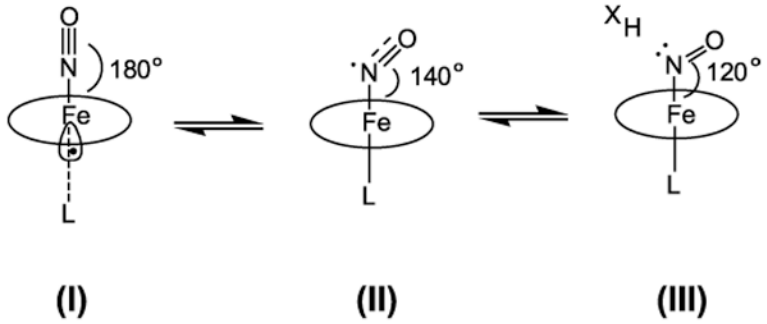

Figure 11.
Valence isomers of LFeP(NO). Although formal charges on NO are + for (I) and − for (II), these are compensated by greater backbonding in (I). However negative charge builds up on N in (III), and is stabilized by appropriately oriented H-bonds, as in MbNO.

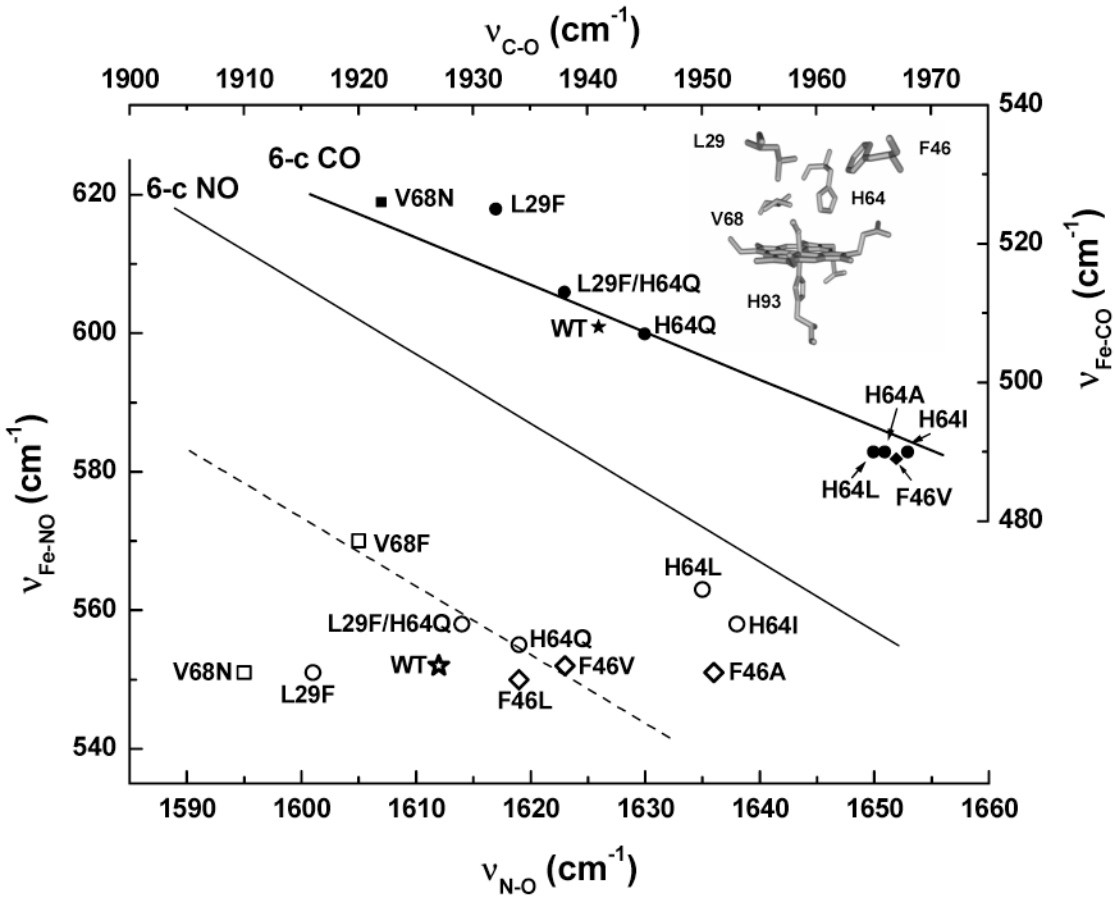

Figure 12.

vFeX/vXO plot for the indicated variants of Mb: WT (stars), H64X (circles), L29F (circles), V68X (squares) and F46X (diamonds). The open symbols represent $Fe^{II}NO$ adducts; closed symbols are $Fe^{II}CO$ adducts. The solid lines are the backbonding correlations for 6-c protein free XO adducts (from Figure 5). The inset shows the positions of mutated distal residues in the Mb binding pocket (49).

Table 1

Experimental vibrational frequencies and isotopic shifts for (N-MeIm)Fe^{II}(TPP-Y)(L)(XO) complexes with indicated phenyl substituent, Y

Substituent (Y) (Solvent)	ν(Fe-N) (cm^{-1})	$\Delta^{15}N$	ν(Fe-C) (cm^{-1})	$\Delta^{13}C$	ν(N-O) (cm^{-1})	$\Delta^{15}N$	ν(C-O) (cm^{-1})	$\Delta^{13}C$
p-OH (DMF)			501	4			1953	45
p-OCH_3 (CH_2Cl_2)	587	22	498	3	1621	33	1960	45
p-CH_3 (CH_2Cl_2)	586	18			1622	31		
H(CH_2Cl_2)	582	15	495	3	1623	32	1962	46
2,6-Cl_2 (CH_2Cl_2)	576	23			1630	30		
2,6-F_2 (CH_2Cl_2)	574	21			1632	32		
F_5 (CH_2Cl_2)	577	23			1632	29		
p-NO_2 (DMF)			492	3			1966	45

J Am Chem Soc. Author manuscript; available in PMC 2008 September 5.

Table 2

Backbonding parameters* for Fe(II) porphyrin NO and CO adducts

	ν°(Fe-C) (cm^{-1})	**Slope (s)**	**ν°(Fe-N) (cm^{-1})**	**Slope (s)**
Experimental				
Five-coordinate	435	-0.46	445	-0.40
Six-coordinate	371	-0.68	329	-1.0
DFT-calculated				
Five-coordinate	534	-0.58	-	-
Six-coordinate	443	-0.82	523	-0.37

* $\nu FeX = \nu°FeX - s[\nu XO - \nu°XO]$; $\nu°XO$ (gas phase) = 2145cm^{-1} for CO and 1876cm^{-1} for NO.

Table 3

Experimental and Computed structural parameters for 5-C and 6-C FeXO adducts

compound	Fe-XO(Å)	X-O(Å)	Fe-X-O (deg)	Fe-L(Å)[a]	Fe-Np(Å)[b]	ref
			Five-coordinate CO			
Fe(Deut)(CO)(THF)[c]	1.706(5)	1.144(5)	177.4(9)	2.127(4)	1.980	20
calc: FeP(CO)[d]	1.735	1.152	180.0		2.008	t.w.
			Six-coordinate CO			
(N-MeIm)Fe(TPP)(CO)[e]	1.7600(17)	1.139(2)	177.03(15)	2.0503(14)	2.005(6)	22
calc: (ImH)FeP(CO)[d]	1.796	1.150	180.0	2.082	2.024/2.026	t.w.
			Five-coordinate NO			
Fe(TPP)(NO)	1.717(7)	1.122(12)	149.2(6)		2.001(3)	23
Fe(TpivPP)(NO)[f]	1.716(15)	1.197(9)	143.8		1.981(26)	24
<Fe(Por)(NO)>[g]	1.728(5)	1.168(1)	143.4(9)		2.008(3)	21
calc: FeP(NO)[h]	1.716	1.196	142.5		2.044/2.015*	t.w.
			Six-coordinate NO			
(N-MeIm)Fe(TPP)(NO)[e]	1.750(2)	1.182(3)	137.7(2)	2.173(2)	2.008(13)	21
(Py)Fe(TpivPP)(NO)[f]	1.742(5)	1.194(9)	133.4(5)	2.260(5)	2.009(2)	21
<(L)Fe(Por)(NO)>[h]	1.752(4)	1.174(6)	138.5(11)		2.007	21
calc: (ImH)FeP(NO)[h]	1.749	1.199	139.3	2.236	2.046/2.026*	t.w.

[a] L – trans axial ligands;

[b] Np – pyrrole N;

[c] Deut – deuteroporphyrin IX, THF – tetrahydrofuran (solvent);

[d] B3LYP functional, VTZ basis set;

[e] N-MeIm – N-methylimidazole, TPP – tetraphenylporphyrin;

[f] TpivPP – tetrakis(o-pivalamidophenyl)porphyrin;

[g] "canonical" values reported by Scheidt;

[h] BLYP functional, VTZ basis set.

* Fe-Np bonds directed away from/towards the FeNO bending (Fig. 6)

Table 4

Experimental and computed frequencies and main potential energy contributions to FeXO modes of Fe(II)NO and Fe(II)CO porphyrins

	Experimental		Calculated					
			CO		NO			
	Fe(TPP)(CO) (cm^{-1})	Fe(TPP)(NO) (cm^{-1})	ν (cm^{-1})	PED (%)[a]	ν (cm^{-1})	PED (%)	$\Delta^{54/57}$Fe (cm^{-1})	$\Delta^{14/15}$N (cm^{-1})
Five-coordinate								
δFeXO			510	65	425	32%	3.7	3.0
νFe-XO	525[b]	524[c]	561	88	599	95%	4.5	10.4
νX-O	1951[b]	1678[c]	2101	97	1686	96%	0.1	32.0
Six-coordinate								
δFeXO		451[d]	568/573	51/52	472	31% δFeNO 29% νFe-NO	5.8	2.9
νFe-XO	495[e]	582[e]	474	84	602	66% νFe-NO 21% δFeNO	2.6	14.8
νX-O	1962[e]	1623[e]	2111	97	1669	97%	0	31.2

[a] Percentage contribution of the indicated internal coordinate to the potential energy of the computed mode;

[b] ref. 3;

[c] ref. 2;

[d] ref. 10;

[e] this work.

Table 5

Vibrational frequencies for 6-c Fe(II)-XO heme proteins

Proteins	ν(Fe-N) (cm^{-1})	ν(Fe-C) (cm^{-1})	ν(N-O) (cm^{-1})	ν(C-O) (cm^{-1})	ref
AXCP	579	491	1624	1966	37
RCCP	569	494	1625	1966	38
BjFixLH	568	497	1634	1967	39
AxPDEA1H	560	493	1637	1973	39
EcDosH	563	487	1632	1969	39
MtDosH	567	494	1639	1972	39
TtTar4H	553	490	1655	1989	40
CcO (*T. t.*)	539	507	1620	1973	41, 42
Cgb	569	492	1604	1971	43
Ngb	573	494	1600	1972	43
WT-Mb	552	508	1612	1941	9
H64L-Mb	563	490	1635	1965	9
H64I-Mb	558	490	1638	1968	9
P450cam	554	474	1591	1955	44,45,34

Table 6

Angle Dependence of (ImH)Fe^{II}P(NO): frequencies (cm^{-1}), distances (Å), energies (kcal/mol) and atomic charges (z).

Angle (°)	**129**	**139**	**149**
νFeN	576	602	600
νNO	1634	1669	1697
δFeNO	467	471	474
d(Fe-N)	1.775	1.749	1.734
d(N-O)	1.202	1.199	1.196
d(Fe-Im)	2.230	2.236	2.247
ΔE	1.42	0	1.23
z_N	-0.019	-0.005	+0.007
z_O	-0.178	-0.195	-0.212